2) Ito, S. and K. Ogawa: *J. Chem. Eng. Japan*, **6**, 231 (1973).
3) Ito, S., K. Ogawa and T. Yuhara: *Kagaku Kōgaku*, **37**, 698 (1973).
4) Ogawa, K., C. Kuroda and S. Yoshikawa: *J. Chem. Eng. Japan*, **18**, 544 (1985).
5) Ogawa, K., C. Kuroda and S. Yoshikawa: *J. Chem. Eng. Japan*, **19**, 345 (1986).

FORMATION OF NICKEL CONCENTRATION PROFILE IN NICKEL/ALUMINA CATALYST DURING POST-IMPREGNATION DRYING

YOSHIMITSU UEMURA, YASUO HATATE AND ATSUSHI IKARI
Department of Chemical Engineering, Kagoshima University, Kagoshima 890

Key Words: Mass Transfer, Nickel Concentration Profile, Nickel Alumina Catalyst, Impregnation, Electron Probe Microanalysis, Solute Migration Model

Nickel concentration profiles were studied for impregnated nickel/alumina catalysts prepared by impregnating two types of spherical aluminas with nickel (II) chloride aqueous solution and applying a wide range of post-impregnation drying conditions. Migration of nickel (II) ion towards the outer surface of alumina occurred during post-impregnation drying. The fraction of migrated nickel (II) ion increased with increase of the constant drying rate, and was held at a constant value, 0.5, at values of the constant drying rate larger than 2×10^{-4} kg·m^{-2}·s^{-1}.

A model of solute migration during post-impregnation drying, combining solution movement by a capillary force with solute diffusion, was proposed. The observed nickel concentration profiles of the nickel/alumina catalysts showed good agreement with the results calculated by the model over the whole range of drying conditions.

Introduction

Impregnation is one of the most important industrial methods of preparing supported catalysts. Since Maatman[10,11] introduced the concept of movement of an active material precursor within supports during impregnation, many studies[5,6,9,16] of the phenomena have been reported. Recently, the majority[1,7,14] of such studies are concerned with control of the profile of an active material precursor. It seems that the techniques to obtain a desired concentration profile of an active material precursor during impregnation are established to some extent. However, the profile formed during impregnation may be destroyed by post-impregnation drying, which causes migration of an active material precursor toward the outer surface of supports, i.e., surface segregation.[4,7,15]

Kotter *et al.*[8] reported that addition of hydroxyethylcellulose to the impregnating solution depressed the surface segregation. However, the decrease of penetration rate of the impregnating solutions due to viscosity increase makes the technique a restricted one. To solve such a problem, quantitative investigation of the surface segregation of an active material precursor is preferable, but no model for interpreting that phenomenon quantitatively has been found.

In the present study, the effects of the post-impregnation drying conditions on the nickel concentration profiles of impregnated nickel/alumina catalysts were investigated by impregnating two types of spherical aluminas with nickel (II) chloride aqueous solution and applying a wide range of drying conditions. Furthermore, a model of solute migration during post-impregnation drying is proposed to describe the nickel concentration profiles.

1. Experimental

1.1 Preparation of catalysts

Eighteen kinds of impregnated nickel/alumina catalysts were prepared by using two types of aluminas (JRC-ALO-1 and JRC-ALO-3 supplied by Catalysis Society of Japan) and applying nine kinds of post-impregnation drying conditions. The typical properties of the supports and the preparation conditions are presented in **Table 1**.

1) Impregnation Spherical aluminas of average diameter about 3 mm were impregnated with nickel

Received June 30, 1986. Correspondence concerning this article should be addressed to Y. Uemura.

Table 1. Experimental conditions

Support		JRC-ALO-1	JRC-ALO-3
form		white sphere	white sphere
composition[3]		$\eta+\gamma$-alumina	γ-alumina
BET surface area[2]	[$m^2 \cdot kg^{-1}$]	1.69×10^5	1.21×10^5
modal pore diameter[3]	[nm]	9.0	10.0
specific pore volume[3]	[$m^3 \cdot kg^{-1}$]	6.70×10^{-4}	5.28×10^{-4}
intrinsic density	[$kg \cdot m^{-3}$]	3.29×10^3	3.43×10^3
porosity	[—]	0.688	0.644
average diameter	[mm]	3.4	3.3
nickel ads. n_0	[$mol \cdot kg^{-1}$]	0	0.194
nickel ads. K	[$l \cdot mol^{-1}$]	—	236
Impregnation		$NiCl_2$ aq. solution (308 K)	
support weight	[kg]	0.042	0.007
impregnant volume	[l]	0.100	0.100
initial conc.	[$mol \cdot l^{-1}$]	0.237	0.040
final conc.	[$mol \cdot l^{-1}$]	0.237	0.027
Drying		under flowing nitrogen gas	
drier I.D.	[cm]	2.60	
gas flow rate	[l-STP$\cdot h^{-1}$]	0.6, 12, 45	
temperature	[K]	333, 373, 673	
Reduction		under flowing hydrogen gas (673 K, 4 h)	

(II) chloride aqueous solution till the adsorption equilibrium of nickel (II) ion was reached. As shown in Table 1, ALO-1 adsorbs no nickel (II) ion, whereas ALO-3 adsorbs to the extent of 0.194 $mol \cdot kg^{-1}$ as a saturated amount. In the final stage of impregnation, the fraction of the nickel (II) ion dissolved in the pore solution to the total nickel is 100% for ALO-1 (nickel (II) ion nonadsorptive alumina), and is 8% for ALO-3 (nickel (II) ion adsorptive alumina).

2) Drying and reduction After impregnation, the impregnated aluminas were dried in a stream of nitrogen gas by the drying apparatus shown in **Fig. 1**. The drying apparatus consists of gas flow rate control sections for drying (1, 3, 4) and for dilution (2, 3, 4), a drier (8), and a humidity detector (11, 12). The drier (8) is a Pyrex glass tube of internal diameter 2.60 cm, in which a sample holder (7) made by stainless net is suspended using the sleeve of the thermocouple. The inner temperature of the drier (8) is maintained at a desired value by an electric furnace (5) and a temperature controller (10). To prevent one-side drying, the impregnated support in the holder (7) is rotated slowly by a vibrator (6) during the drying. After attaining desired gas flow rate and temperature, about 600 mg of the impregnated support was charged from the top of the drier. The relative humidity of effluent gas was monitored continuously by the detector during the drying. When no humidity was detected, drying was terminated. The drying rate was calculated from the relative humidity and the gas flow rate.

The dried samples were reduced in a stream of hydrogen gas of 100 $cm^3 \cdot min^{-1}$ at 673 K for 4 h.

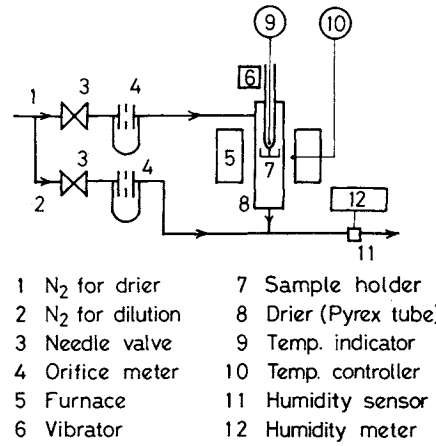

Fig. 1. Schematic diagram of drying apparatus.

1.2 Nickel concentration profile

Nickel concentration profiles along the diameter of the catalyst cross section were measured by electron probe microanalyser (EPMA, Shimadzu ARL microprobe X-ray analyser). The catalyst was imbedded in a thermoplastic resin. After solidification, sand papers (No. 220, 600, and 1500) were used to grind off the catalyst particles to expose the cross section. For fine polishing, a liquid polishing agent containing fine diamond powders was used. The sample was coated with a layer of carbon by vacuum deposition. The acceleration voltage of the electron beam was 15 kV and the scanning speed was 0.02 $mm \cdot min^{-1}$.

2. Results and Discussion

2.1 Effect of drying rate on nickel concentration profile

In **Fig. 2**, a nickel concentration profile (*) of the catalyst, prepared by drying the impregnated spherical ALO-1, is compared with that (**) of the catalyst, prepared by drying the slab-form sample of 0.5 mm thickness sectioned before drying. The result indicates that the nickel concentration profile of the impregnated alumina (profile (**) in Fig. 2) is uniform,[7] and that of the dried sample (profile (*) in Fig. 2) becomes nonuniform by the migration of nickel during post-impregnation drying.

In **Figs. 3** and **4**, nickel concentration profiles and drying rate diagrams as a function of moisture for various post-impregnation drying conditions are given using ALO-1 and ALO-3, respectively. The catalysts prepared by using ALO-1 (Fig. 3) show surface segregation of nickel, the extent of which increases with increasing drying rate. The catalysts prepared by using ALO-3 (Fig. 4) show uniform profiles almost independent of the drying rate. The difference of nickel (II) ion adsorption capacity between ALO-1 and ALO-3, as described in Section 1.1, is responsible for such a difference.

In **Fig. 5**, the fractions of nickel (II) ion migrated

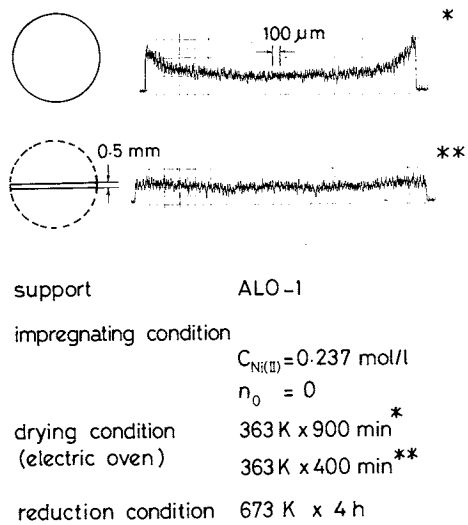

Fig. 2. Nickel migration in spherical alumina during drying (EPMA response profiles).

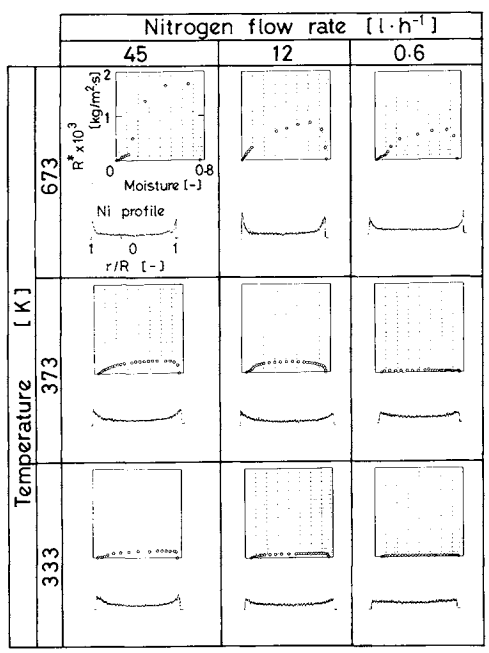

Fig. 3. Effect of drying rate on nickel concentration profile (alumina: JRC-ALO-1).

during the drying to the total nickel (fraction of migrated nickel) are plotted against the constant drying rates to study the nonuniformity of the nickel concentration profiles of the catalysts prepared by using ALO-1 presented in Fig. 3. The constant drying rates were obtained from the plateaus in the drying rate diagrams. Since the nickel concentration profiles of the catalysts by using ALO-1 (Fig. 3) are concave curves, which are minimum at the center of the catalyst particle, the fraction of migrated nickel is calculated from the following equation.

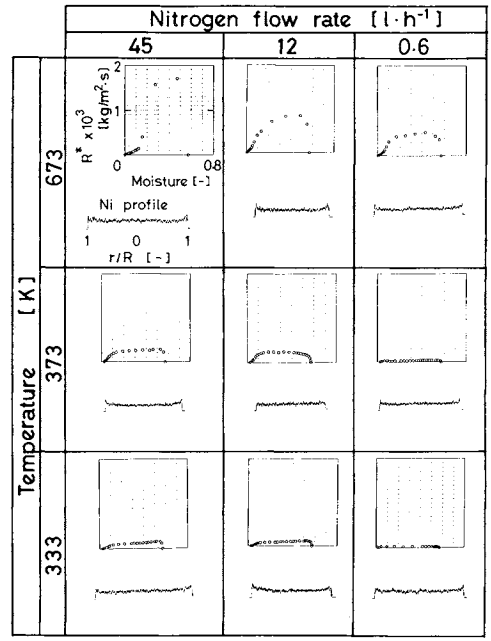

Fig. 4. Effect of drying rate on nickel concentration profile (alumina: JRC-ALO-3).

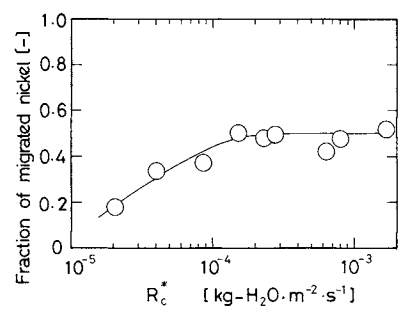

Fig. 5. Effect of drying rate on fraction of migrated nickel (alumina: JRC-ALO-1).

$$f_m = \frac{\int_0^1 \{w(x) - w(0)\} x^2 dx}{\int_0^1 w(x) x^2 dx} \tag{1}$$

where the nickel concentration profiles shown in Fig. 3 are used as $w(x)$. In Fig. 5, the fraction of migrated nickel, f_m, increases with increase in the constant drying rate in the rate range from 2×10^{-5} to 2×10^{-4} kg·m^{-2}·s^{-1}, and is maintained at a constant value, 0.5, at values of the constant drying rate larger than 2×10^{-4} kg·m^{-2}·s^{-1}. The result indicates that the fraction of migrated nickel during drying shows an upper limiting value.

2.2 A model of solute migration during drying

Though the surface segregation of an active material precursor during drying has been reported by many workers,[4,7,15] no quantitative model to interpret the phenomena has been found. Komiyama *et al.*[7] indicated qualitatively that a capillary force would be related to the surface segregation. To

interpret the surface segregation quantitatively, the authors propose a model of solute migration during the drying that considers solution movement by a capillary force and solute diffusion.

1) Modeling of solution movement during drying **Figure 6** illustrates a general aspect of solution movement within a porous support during drying which involves constant rate period and falling rate period. In the initial stage of drying, evaporation occurs from the all menisci facing the outer surface of a support (Fig. 6(a)). After a moment, the solution moves from the comparatively large pore ("macro" pore) to the comparatively small pore ("micro" pore) by capillary force. The moving solution flows in "micro" pore from the inside to the outer surface of the support (Figs. 6(b) and 6(c)). In these stages, the drying rate is observed to be constant. In a further developed stage, the solution within "macro" pore is exhausted and the funicular solution within "micro" pore becomes the wedge solution (Fig. 6(d)). Instantaneously, solution movement within "micro" pore is substantially terminated.

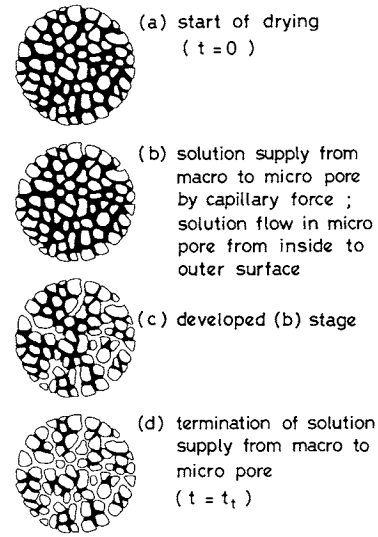

Fig. 6. General aspect of solution movement during drying.

In **Fig. 7**, a proposed model of solution movement during constant drying is illustrated. In this model, we assume the following for simple treatment: (1) the impregnated support is spherical; (2) the impregnated support is kept isothermally at wet-bulb temperature; (3) the solvent evaporates from only the menisci facing the outer surface of the support; (4) the density of solution within the pore is constant independent of concentration and equals that of the solvent; (5) "macro" pore works as a reservoir tank, which supplies solution of concentration C_0 into "micro" pore; (6) the supplying rate is proportional to the volume element of a spherical shell ($4\pi r^2 dr$).

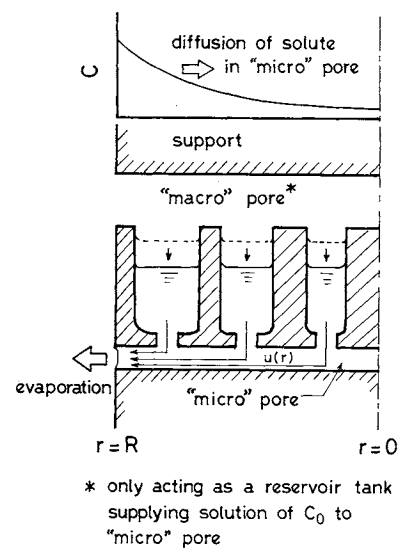

Fig. 7. Model of solution movement.

The velocity of the solution in "micro" pore at the outer surface is expressed as the following equation, derived from the mass balance of the solvent at $r=R$.

$$u_R=\frac{R_c^*}{\varepsilon_i\rho_s} \tag{2}$$

The velocity of the solution in "micro" pore is derived from the mass balance of the solution in the differential shell.

$$u=u_R\frac{r}{R} \tag{3}$$

The termination time of solution supply from "macro" pore to "micro" pore is given by the following expression.

$$t_t=\frac{\varepsilon_a R}{3\varepsilon_i u_R} \tag{4}$$

2) A solute migration model Solute migration within a support is caused not only by the solution movement described in the preceding section but also by diffusion due to concentration gradients caused by the evaporation of the solvent at $r=R$. The following equation is derived from the mass balance of a solute in the differential shell, in which "macro" pore works as a reservoir tank supplying solution of concentration C_0 to "micro" pore.

$$D_e\left(\frac{\partial^2 C}{\partial r^2}+\frac{2}{r}\frac{\partial C}{\partial r}\right)-\frac{\varepsilon_i u_R}{R}\left\{r\frac{\partial C}{\partial r}+3(C-C_0)\right\}=\varepsilon_i\frac{\partial C}{\partial t} \tag{5}$$

The initial condition is

$$t=0;\quad C=C_0 \tag{6}$$

The boundary conditions are

$$r=0;\quad \frac{\partial C}{\partial r}=0 \tag{7}$$

$$r=R\,;\quad D_e\frac{\partial C}{\partial r}=\varepsilon_i u_R C \tag{8}$$

By introducing

$$x=r/R;\quad c=C/C_0;\quad \theta=tD_e/(\varepsilon_i R^2);$$
$$u_0=R_c^* R/(\rho_s D_e)$$

Eqs. (5), (6), (7) and (8) become

$$\frac{\partial^2 c}{\partial x^2}+\frac{2}{x}\frac{\partial c}{\partial x}-u_0\left\{x\frac{\partial c}{\partial x}+3(c-1)\right\}=\frac{\partial c}{\partial \theta} \tag{9}$$

$$\theta=0;\quad c=1 \tag{10}$$

$$x=0;\quad \frac{\partial c}{\partial x}=0 \tag{11}$$

$$x=1;\quad \frac{\partial c}{\partial x}=u_0 c \tag{12}$$

Dimensionless termination time is

$$\theta_t=\frac{\varepsilon_a}{3\varepsilon_i u_0} \tag{13}$$

Eqs. (9), (10), (11) and (12) are characterized by the parameter u_0, which is determined from the ratio of $R_c^*$to D_e. In the present model, the solute migration in "micro" pore is expressed by Eqs. (9), (10), (11) and (12) until solution supply from "macro" pore terminates. The solute migrates in "micro" pore by solution flow and diffusion. At the termination time, solute migration in the support substantially terminates, because the funicular solution within "micro" pore becomes the wedge solution. Hence, the concentration profile of an active material precursor is established. The solution of Eqs. (9), (10), (11) and (12) at θ_t expresses the final concentration profile of an active material precursor. In the application of this model, Fick's law and constant density of the solution should be approximated.

3) Comparison with experimental results The parameters of the model calculation are presented in **Table 2**. As shown in Fig. 5, the porosity of "macro" pore approximately equals that of "micro" pore at values of constant drying rate larger than $2\times10^{-4}\,\mathrm{kg\cdot m^{-2}\cdot s^{-1}}$. Each porosity of ALO-1 was calculated as follows:

$$\varepsilon_i=0.5\varepsilon\,,\quad \varepsilon_a=0.5\varepsilon \tag{14}$$

The parameters, ε_i and ε_a, are assumed to be expressed by Eq. (14) in the drying rate range from 2×10^{-5} to $2\times10^{-4}\,\mathrm{kg\cdot m^{-2}\cdot s^{-1}}$.

In **Figs. 8, 9** and **10**, the observed nickel concentration profiles of the catalysts using ALO-1 (white and black keys in these figures) are compared with the results of the model calculation (solid lines). Both profiles are expressed as a normalized form to make a clear comparison. As shown in Figs. 8, 9 and 10, the two profiles are in good agreement.

Table 2. Model parameters for calculation of nickel concentration profile

R_c^* [$\mathrm{kg\cdot m^{-2}\cdot s^{-1}}$]	$2.1\times10^{-5}\sim1.7\times10^{-3}$	*
D [$\mathrm{m^2\cdot s^{-1}}$]	$1.4\times10^{-9}\sim4.8\times10^{-9}$	**
D_e [$\mathrm{m^2\cdot s^{-1}}$]	$8.0\times10^{-11}\sim2.8\times10^{-10}$	***
ε_i [—]	0.344	
ε_a [—]	0.344	
τ_i [—]	6[13]	
ρ_s [$\mathrm{kg\cdot m^{-3}}$]	1.0×10^3	
R [m]	1.7×10^{-3}	

* Experimental value.
** Calculated from the Nernst-Haskell equation at wet-bulb temperature.[12]
*** $D_e=\frac{\varepsilon_i}{\tau_i}D$.

Since the fraction of nickel (II) ion dissolved in the pore solution to the total nickel (II) ion content of the impregnated ALO-3 is 8% as described in Section 1.1, almost uniform nickel concentration profiles may be expected for the nickel/ALO-3 catalysts. This expectation is consistent with the observed nickel concentration profiles of the nickel/ALO-3 catalysts (Fig. 4).

The above discussion shows that the present model is applicable to predict the concentration profile of an active material precursor after post-impregnation drying over a wide range of drying conditions. The parameters (u_0, ε_i and ε_a), suggested in the present model, give a criterion for predicting the extent of surface segregation of an active material precursor. Direct measurements are possible for R_c^*, R and ρ_s. Diffusion coefficient of solute, D_e, can be estimated from the Nernst-Haskell equation.[12] The ratio of ε_i to ε_a can be measured by the method mentioned in the experimental section.

Conclusion

The nickel concentration profiles of impregnated nickel/alumina catalysts were studied by using two types of aluminas and applying a wide range of post-impregnation drying conditions. The following conclusions were drawn from the results and discussion above.

1) Nickel segregation toward the outer surface of the support becomes significant with increasing post-impregnation drying rate. The fraction of migrated nickel increases with increase in constant drying rate up to an upper limiting value, 0.5. Such migration is negligible in the case where the adsorbed nickel (II) ion is predominant.

2) A solute migration model, combining the solution movement by capillary force with solute diffusion, gave a good interpretation of the observed nickel concentration profiles of catalysts prepared over a wide range of drying conditions.

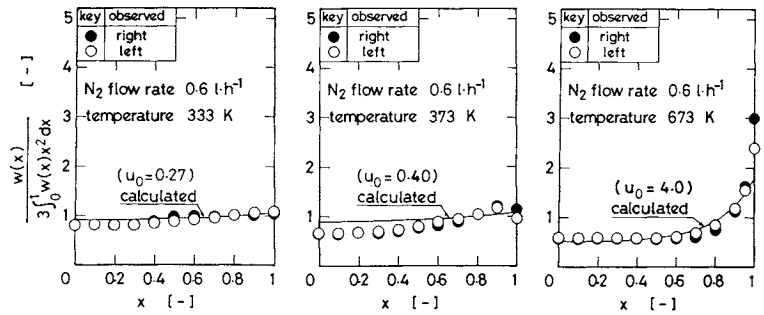

Fig. 8. Comparison of observed nickel concentration profile with calculated value (nitrogen flow rate: $0.6\,l \cdot h^{-1}$).

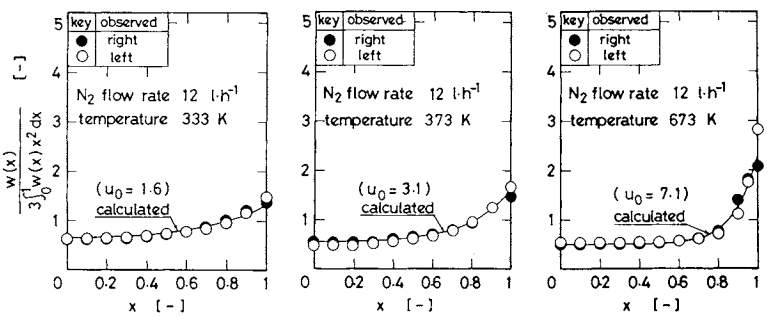

Fig. 9. Comparison of observed nickel concentration profile with calculated value (nitrogen flow rate: $12\,l \cdot h^{-1}$).

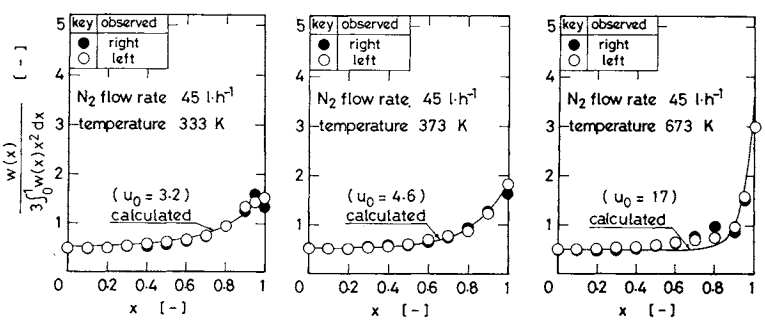

Fig. 10. Comparison of observed nickel concentration profile with calculated value (nitrogen flow rate: $45\,l \cdot h^{-1}$).

Acknowledgment

The authors are very grateful to Professors F. Nakashio and S. Morooka of Kyushu University for their support and advice.

Nomenclature

C	=	concentration of solute	$[mol \cdot m^{-3}]$
C_0	=	concentration of solute before drying	$[mol \cdot m^{-3}]$
c	=	dimensionless concentration defined as C/C_0	[—]
D	=	diffusion coefficient of solute	$[m^2 \cdot s^{-1}]$
D_e	=	effective diffusion coefficient of solute	$[m^2 \cdot s^{-1}]$
f_m	=	fraction of migrated nickel defined in Eq. (1)	[—]
K	=	adsorption equilibrium constant of Langmuir isotherm	$[l \cdot mol^{-1}]$
n_0	=	amount of saturation adsorption of Langmuir isotherm	$[mol \cdot kg^{-1}]$
R	=	catalyst particle radius	[m]
R^*	=	drying rate	$[kg \cdot m^{-2} \cdot s^{-1}]$
R_c^*	=	constant drying rate	$[kg \cdot m^{-2} \cdot s^{-1}]$
r	=	radial distance from the center of catalyst particle	[m]
t	=	time	[s]
u	=	velocity of solution in "micro" pore	$[m \cdot s^{-1}]$
u_R	=	velocity of solution in "micro" pore at $r=R$	$[m \cdot s^{-1}]$
u_0	=	dimensionless parameter defined as $R_c^* R/(\rho_s D_e)$	[—]
X	=	moisture	[—]
x	=	dimensionless radial distance defined as r/R	[—]
$w(x)$	=	local concentration of active component of catalyst as a function of x	[wt%]
ε	=	porosity	[—]
θ	=	dimensionless time defined as $tD_e/(\varepsilon_i R^2)$	[—]
ρ_s	=	density of solution	$[kg \cdot m^{-3}]$
τ	=	tortuosity factor	[—]

〈Subscripts〉

a	=	"macro" pore

i = "micro" pore
t = termination time of macro-scale migration of solute

Literature Cited

1) Becker, E. R. and T. A. Nuttall: Preprints for the Second International Symposium on Scientific Bases for the Preparation of Heterogeneous Catalysts, B-5 (1978).
2) Data-JRC-0001, Hattori, T.: *Shokubai (Catalyst)*, **22**, 115 (1980).
3) Data-JRC-0002, Mukaida, K.: *Shokubai (Catalyst)*, **22**, 116 (1980).
4) Galiasso, R., O. L. de Ochoa and P. Andreu: *Appl. Catal.*, **5**, 309 (1983).
5) Harriott, P.: *J. Catal.*, **14**, 43 (1969).
6) Komiyama, H., T. Kataoka and H. Inoue: *Kagaku Kogaku Ronbunshu*, **10**, 337 (1984).
7) Komiyama, M., R. P. Merrill and H. F. Harnsberger: *J. Catal.*, **63**, 35 (1980).
8) Kotter, M. and L. Riekert: Preprints for the Second International Symposium on Scientific Bases for the Preparation of Heterogeneous Catalysts, A-4 (1978).
9) Lee, H. H.: *Chem. Eng. Sci.*, **39**, 859 (1984).
10) Maatman, R. W.: *Ind. Eng. Chem.*, **51**, 913 (1959).
11) Maatman, R. W. and C. D. Prater: *Ind. Eng. Chem.*, **49**, 253 (1957).
12) Reid, R. C., J. M. Prausnitz and T. K. Sherwood: "The Properties of Gases and Liquids," p. 591, McGraw-Hill (1977).
13) Satterfield, C. N.: "Mass Transfer in Heterogeneous Catalysis," p. 39, M.I.T. Press (1970).
14) Shyr, Y.-S. and W. R. Ernst: *J. Catal.*, **63**, 425 (1980).
15) van den Berg, G. H. and H. T. Rijnten: Preprints for the Second International Symposium on Scientific Bases for the Preparation of Heterogeneous Catalysts, C-4 (1978).
16) Vincent, R. C. and R. P. Merrill: *J. Catal.*, **35**, 206 (1974).

ANALYSIS OF KINETIC BEHAVIOR OF TEMPERATURE-SENSITIVE WATER-ABSORBING HYDROGEL

XIA HUANG, HAJIME UNNO, TAKASHI AKEHATA AND OKIHIKO HIRASA

Department of Environmental Chemical and Engineering, Tokyo Institute of Technology, Yokohama 227

Key Words: Separation, Polymer Gel, Hydrogel, Swelling, Shrinking, Phase Transition

Kinetic behavior of a temperature-sensitive water-absorbing gel was analyzed experimentally by using a newly developed water-absorbing polyvinylmethylether gel (PVMEG). The gel showed a volume change phenomenon responding to a temperature change across the temperature of 310 K. It swelled and shrank respectively below and above the transition temperature. A simple mathematical model for the kinetic behavior of the gel is presented and it is found that the simulated behavior of the gel fits very well with the experimental results by employing appropriate values for the parameters included in the model.

Introduction

Polymer hydrogels, such as hydrolyzed acrylamide gel, have been found to show a large volume change responding to an infinitesimal change in external conditions such as temperature, electric field, pH and salt concentration.[3] The volume change, which is referred to as a phase transition, is ascribed to a change in the configuration of the gel matrix.

One of the most popular applications of hydrogels is as a water preservation agent for sanitary and agricultural uses.[5] In addition to these applications, the phase transition phenomena of gels are being applied to various engineering uses such as extraction,[1] chromatographic separation, concentration of protein and solid-liquid separation.[4]

For the engineering applications mentioned above, it is necessary to clarify the kinetic behavior of gels. A kinetic study of gel swelling, which is driven by an osmotic pressure change, has recently been done theoretically by Tanaka and Fillmore[6] for the case of a small spherical polyacrylamide gel. A numerical mathematical model for syneresis of a gel of protein was reported by Van Dijk *et al.*[7] These researches are a start toward understanding the kinetic behavior of hydrogels, but these mathematical treatments are not enough for the engineering application of a gel sensitive to its external environment.

In the present paper, an engineering analysis is made for both the swelling and shrinking behavior of

Received August 2, 1986. Correspondence concerning this article should be addressed to H. Unno. O. Hirasa is at Research Institute of Polymers and Textiles.